

# All-Optical Microwave Filter With High Frequency Selectivity Based on Semiconductor Optical Amplifier and Optical Filter

Enming Xu, Xinliang Zhang, Lina Zhou, Yu Zhang, Yuan Yu, Xiang Li, and Dexiu Huang

**Abstract**—We propose and experimentally demonstrate a novel all-optical microwave filter with high frequency selectivity. It is based on a recirculating delay line (RDL) loop in which a semiconductor optical amplifier (SOA) is followed by a tunable narrowband optical filter and a  $1 \times 2$  10:90 optical coupler. Converted signal used as a negative tap is generated through wavelength conversion employing the cross-gain modulation (XGM) of the amplified spontaneous emission (ASE) spectrum of the SOA. The converted signal circulating in the RDL loop can realize a high quality factor (Q) response after photo-detection. The  $1 \times 2$  10:90 coupler is employed to extract 10% optical power from the loop as output. A frequency response with a high Q factor of 543, a rejection ratio of 40 dB and a shape factor of 15.4 is experimentally demonstrated.

**Index Terms**—Microwave photonics, microwave filter, optical signal processing, semiconductor optical amplifier.

## I. INTRODUCTION

MICROWAVE photonic filters for microwave and radio frequency (RF) signal processing have attracted considerable attention in recent years [1]–[8]. Compared with traditional electronics-based microwave circuits, microwave photonic filters can provide advantages such as low loss, light weight, broad bandwidth, good tunability, and immunity to electromagnetic interference (EMI). Since high frequency selectivity is a key issue in most applications, the realization of microwave bandpass filtering with high quality factor (Q), high stop-band rejection, and small shape factor is required. Various high Q factor filter structures have been reported [9]–[12]. However, none of them can meet all these requirements simultaneously in the optical domain. Approach based on an infinite-impulse response (IIR) microwave photonic filter has demonstrated a high Q factor of 325 [9]; however, the shape factor and the rejection ratio are limited. An extension of this approach, which uses dual-cavities with gain offset [10], has demonstrated a high Q factor of 240 with an improved rejection ratio; however, the shape factor is still limited. Moreover, this

structure is more complex because two erbium-doped fiber amplifiers (EDFAs) and balanced detection should be used, and precise control of the gain offset level and cavity length are required. Recently, approach based on a higher order bandpass filter has demonstrated a good shape factor and the rejection ratio is 50 dB, however, the Q factor is limited to around 100 [11]. Approach based on stimulated Brillouin scattering shows a high Q factor of 670, however, the filter is complicated and has a limited rejection ratio [12]. These drawbacks have limitations in some applications.

In this paper, we propose and experimentally demonstrate a stable microwave filter which can realize high frequency selectivity in the optical domain. It is based on a recirculating delay line (RDL) loop comprising a semiconductor optical amplifier (SOA), a tunable narrowband optical filter (TNOF) and a  $1 \times 2$  10:90 optical coupler. Converted signal serving as a negative tap is generated through wavelength conversion based on the cross-gain modulation (XGM) of the amplified spontaneous emission (ASE) spectrum of the SOA [13]–[17]. Converted signal circulating in the RDL loop realizes a high Q factor frequency response after photo-detection. The  $1 \times 2$  10:90 coupler is employed to extract 10% optical power from the loop as output, which is different from the previous bandpass filter structures. The residual pump signal not being filtered out by the TNOF realizes a weak all-pass response which makes the shape factor better. This novel filter structure can achieve high frequency selectivity, i.e., high Q factor, high rejection ratio, and good shape factor simultaneously. The experimental results show a high Q factor of 543, a rejection ratio of 40 dB, and a shape factor of 15.4.

## II. EXPERIMENTAL SETUP AND OPERATION PRINCIPLES

### A. Principles of Proposed Novel Filter

The experimental setup of the novel SOA-based microwave bandpass filter is shown in Fig. 1. The output of a laser diode at wavelength of 1551.12 nm is externally modulated by a Mach–Zehnder modulator (MZM) which is driven by a microwave signal from the output port of a vector network analyzer (VNA). The power of the modulated optical signal is controlled by the following EDFA and optical tunable attenuator. Then it is launched into the RDL loop consisting of a  $2 \times 2$  50:50 coupler (OC1) and a SOA followed by a TNOF and a  $1 \times 2$  10:90 optical coupler (OC2). The SOA can be treated as a broadband optical source in the absence of input pump signal, and its spectrum is shown as the upper trace in Fig. 2. On the

Manuscript received October 11, 2009; revised December 18, 2009, January 11, 2010, and January 28, 2010; accepted February 24, 2010. Date of publication March 25, 2010; date of current version August 04, 2010. This work was supported in part by the National Basic Research Program of China under Grant No. 2006CB302805 and the Program for New Century Excellent Talents in Ministry of Education of China under Grant No. NCET-04-0715.

The authors are with Wuhan National Laboratory for Optoelectronics, School of Optoelectronic Science and Engineering, Huazhong University of Science and Technology, 470074 Wuhan, China (e-mail: xlzhang@mail.hust.edu.cn; enmingxu@gmail.com).

Digital Object Identifier 10.1109/JLT.2010.2045102

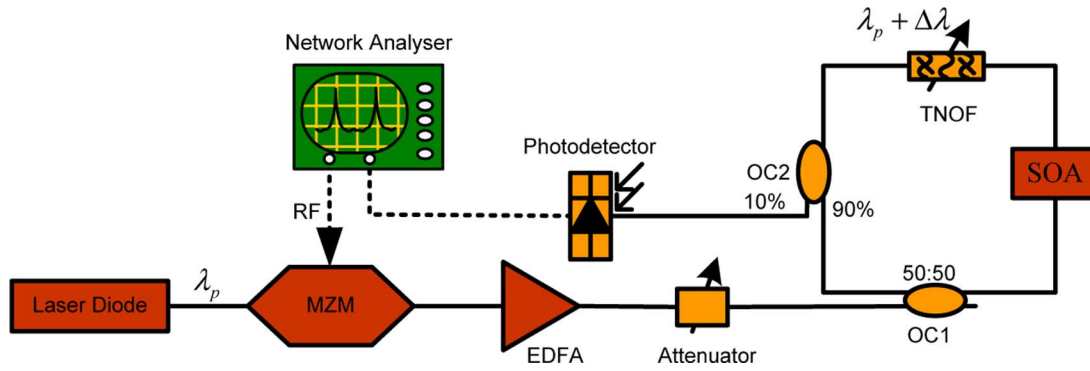


Fig. 1. Experimental setup of novel SOA-based microwave bandpass filter. MZM: Mach-Zehnder modulator, EDFA: erbium-doped fiber amplifier, OC: optical coupler, SOA: semiconductor optical amplifier, TNOF: tunable narrowband optical filter, RF: radio frequency.

contrary, under the condition of the pump signal being injected, the ASE spectrum of the SOA is inversely modulated by the pump signal ( $\lambda_p$ ) due to the XGM effect, and then the modulation information at pump wavelength  $\lambda_p$  is inversely copied into the whole ASE spectrum, and the modulated ASE spectrum of the SOA is shown as the lower trace in Fig. 2. The TNOF with a 3 dB bandwidth of 0.3 nm can extract out the converted signal ( $\lambda_c$ ) at a central wavelength different from that of the pump signal. The extracted converted signal is an inverted copy of the pump signal and is used as a negative tap. A  $1 \times 2$  10:90 coupler is employed to extract 10% optical power from the RDL loop; and the residual 90% power is amplified by the SOA and delayed by the loop to obtain subsequent recursive taps. When the converted signal circulates in the RDL loop, it cannot modulate the ASE spectrum of the SOA again due to its low power, and it is only amplified by the SOA. Thus, the converted signal can circulate in the RDL loop to realize a high Q factor response ( $Q = \text{FSR} / \Delta f_{3\text{ dB}}$ , where FSR is the free spectral range,  $\Delta f_{3\text{ dB}}$  is the 3 dB bandwidth, and  $\text{FSR} = 1/T$ ,  $T$  is the delay time of the loop). On the other hand, since the TNOF has a Gaussian shape and a limited rejection ratio, the pump signal cannot be filtered out completely by the TNOF when the central wavelength of the TNOF is a certain detuning from the input signal wavelength. However, since the SOA is saturated, the weak residual pump signal passing through the TNOF cannot be effectively amplified by the SOA, that is to say, the pump signal passes through the RDL loop only once for contributing to the output. After the first tap of the converted signal is subtracted by the residual pump signal, the subtraction is further combined with the subsequent recursive taps of the converted signal at the output of OC2. Thus, the frequency response of the proposed microwave photonic filter can be considered to be the combination of a weak all-pass response and a high Q factor response with negative coefficients after photo-detection. Finally, the frequency response is measured by the other port of the VNA.

The advantage of this novel filter structure is that the modulated ASE signal circulating in the active loop can realize high Q factor, high rejection ratio, and good shape factor simultaneously in the optical domain and exhibit a very stable operation. For the convenience of further analysis, here, the shape factor is defined as the ratio of the 3 dB bandwidth  $S$  over the maximal rejection level to the 3 dB bandwidth  $B$ , that is  $S/B$ , as shown

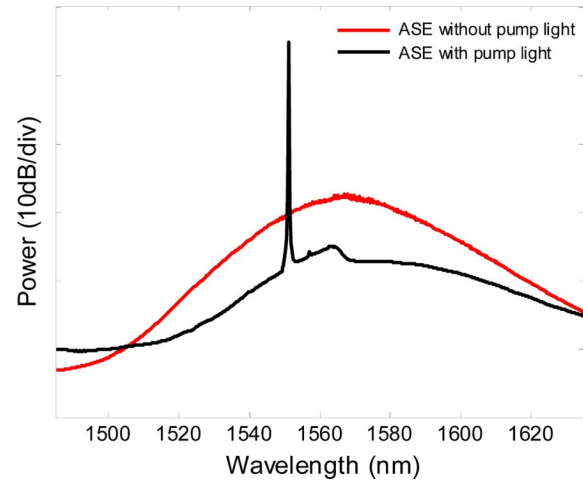


Fig. 2. Optical ASE spectrum of the SOA without and with pump signal at 1551.12 nm wavelength.

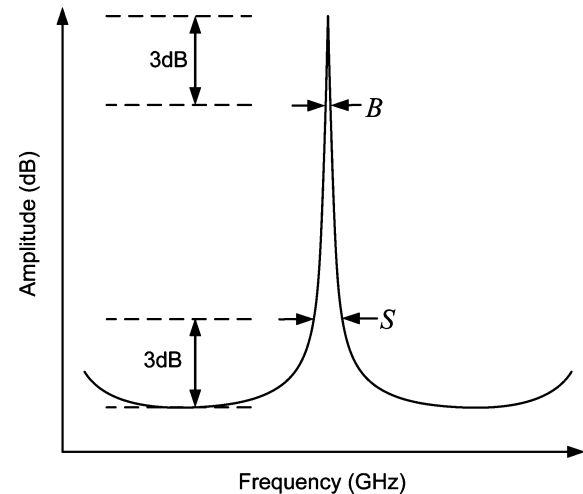


Fig. 3. The general shape of the frequency response of a bandpass filter.

in Fig. 3, which shows the general shape of the frequency response of a bandpass filter. The ideal value of the shape factor equals one.

To analyze the novel filter structure, a theoretical model is presented. If the MZM is operated in the nearly linear region,

the MZM acts as a linear intensity modulator. Assuming an electrical signal  $\cos(\omega t)$  is applied to the MZM, under small-signal conditions, the transmitted optical power  $P_m$  is related to the input optical power  $P_i$  by

$$P_m = \frac{P_i}{2} [1 + m \cos(\omega t)] \quad (1)$$

where  $m$  is the modulation index and  $\omega$  is the angular frequency of the electrical signal.

Assuming the filter structure is operated in the incoherent regime, the power of the residual pump signal is given by

$$P_p = \frac{GLP_i}{2} [(1 - \kappa_1)(1 - \kappa_2)g_p L_p (1 + m \cos(\omega t))] \quad (2)$$

where  $G$  is the gain of the EDFA,  $L$  is the optical loss coefficient of the attenuator,  $\kappa_1$  and  $\kappa_2$  are the coupling ratios of OC1 and OC2, respectively,  $g_p$  is the effective gain of the pump signal by the SOA,  $L_p$  is the optical loss coefficient of the pump signal caused by the TNOF.

For the converted signal circulating in the RDL loop, while neglecting fiber chromatic dispersion, the summation power of all the delayed taps can be written as

$$P_c = \frac{GLP_i}{2} \left\{ \sum_{n=1}^{\infty} \eta(1 - \kappa_1)(1 - \kappa_2)\kappa_1^{n-1}\kappa_2^{n-1}g_c L_c^n \right\} \cdot [1 + m \cos(\omega(t - (n-1)T) + \pi)] \quad (3)$$

where  $\eta$  represents the XGM conversion coefficient of the microwave optical signal from wavelength  $\lambda_p$  to  $\lambda_c$ ,  $g_c$  is the effective gain of the converted signal by the SOA,  $L_c$  is the optical loss coefficient of the converted signal caused by the TNOF,  $T = n_{\text{eff}}l_{\text{act}}/c$  is the delay time corresponding to the RDL loop length  $l_{\text{act}}$ ,  $n_{\text{eff}}$  is the fiber refractive index, and  $c$  is the speed of light in vacuum.

Therefore, the summation power of all the taps of the novel filter structure can be expressed as

$$P = \frac{GLP_i}{2} \left\{ \begin{aligned} &(1 - \kappa_1)(1 - \kappa_2)g_p L_p (1 + m \cos(\omega t)) \\ &+ \sum_{n=1}^{\infty} \eta(1 - \kappa_1)(1 - \kappa_2)\kappa_1^{n-1}\kappa_2^{n-1}g_c L_c^n \\ &\cdot [1 + m \cos(\omega(t - (n-1)T) + \pi)] \end{aligned} \right\} \quad (4)$$

Since we are only interested in AC components, DC components at the PD output is not considered. Applying Fourier transform to both sides of (4), and comparing with the input signal, the transfer function of the filter structure is then obtained in (5), shown at the bottom of the page, where  $K = \Re GLP_i m/2$ .  $K$  is a scale factor that does not affect the shape of the filter frequency response.  $\Re$  is the responsivity of the PD.  $H_1(\omega)$  and

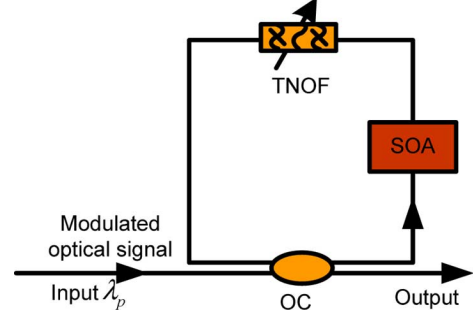


Fig. 4. Schematic scheme of the conventional SOA-based filter.

$H_2(\omega)$  represent the frequency response realized by the residual pump signal and converted signal, respectively.

As can be seen from (5), the overall frequency response of the filter is determined by the coupling coefficients  $\kappa_1, \kappa_2$ , the optical loss coefficients  $L_p, L_c$ , and the SOA effective gains  $g_p, g_c$ . The modulated ASE spectrum has a non-flatten shape, shown as the lower trace in Fig. 2. Therefore, at a given SOA bias current, adjusting the TNOF will induce different  $g_p, g_c$ , thus results in different characteristics of the overall frequency response.

### B. Comparison With Conventional Filter

For the purposes of comparison, the conventional SOA-based filter scheme is shown in Fig. 4 [14], [18]. The conventional filter is with a  $2 \times 2$  50:50 coupler, and the central wavelength of the TNOF is aligned with the pump signal wavelength. Its output is extracted at the  $2 \times 2$  50:50 coupler used to form the loop, and its measured frequency response is shown in Fig. 5. This conventional bandpass filter structure has some drawbacks due to the ASE noise of the SOA, such as a limited Q factor of 193, a limited rejection ratio of 14 dB, and a limited shape factor of 22.6.

However, there are some possibilities to improve the performance of the conventional filter. For example the  $2 \times 2$  50:50 coupler can be substituted by a  $2 \times 2$  10:90 coupler and the 10% port is used as output port, and the central wavelength of the TNOF can be detuned from the pump signal wavelength, referred to as the improved conventional filter which is similar to the proposed filter in Fig. 1. Based on the analysis of the proposed filter, the performance of the improved conventional filter is supposed be similar to that of the proposed filter, i.e., the converted signal circulating in the loop realizes a high Q factor frequency response, and the pump signal passes through the RDL loop only once for contributing to the output. Thus,

$$\begin{aligned} H(\omega) &= \frac{\Re GLP_i m}{2} \left[ \frac{(1 - \kappa_1)(1 - \kappa_2)g_p L_p - \sum_{n=1}^{\infty} \eta(1 - \kappa_1)(1 - \kappa_2)\kappa_1^{n-1}\kappa_2^{n-1}g_c L_c^n e^{-j(n-1)\omega T}}{\sum_{n=1}^{\infty} \eta(1 - \kappa_1)(1 - \kappa_2)\kappa_1^{n-1}\kappa_2^{n-1}g_c L_c^n e^{-j(n-1)\omega T}} \right] \\ &= K \left[ \underbrace{(1 - \kappa_1)(1 - \kappa_2)g_p L_p}_{H_1(\omega)} - \underbrace{\frac{\eta(1 - \kappa_1)(1 - \kappa_2)g_c L_c}{1 - \kappa_1 \kappa_2 g_c L_c e^{-j\omega T}}}_{H_2(\omega)} \right] \quad (5) \end{aligned}$$

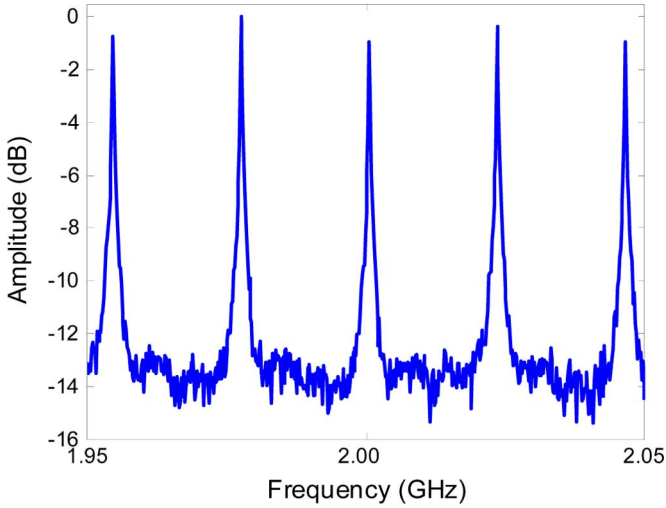


Fig. 5. Measured frequency responses of conventional SOA-based filter with the 50:50 coupler and the central wavelength of the TNOF aligned with pump wavelength.

following a similar procedure to that described for the proposed filter, the transfer function of the improved conventional filter can be written as

$$H'(\omega) = K \left[ \frac{\kappa + (1 - \kappa)^2 g_p L_p e^{-j\omega T}}{\frac{\eta(1-\kappa)^2 g_c L_c e^{-j\omega T}}{1 - \kappa g_c L_c e^{-j\omega T}}} \right] \quad (6)$$

where  $\kappa$  is the coupling ratio of the  $2 \times 2$  coupler.

It can be seen from (5) and (6) that the effects of the pump signal on the filter frequency response are different. In the improved conventional filter, the pump signal realizes a two-tap notch response instead of the all-pass response in the conventional filter. Equation (6) shows that high Q factor frequency response can be achieved if the amplitude of the frequency response realized by the converted signal is much larger than that realized by the pump signal. Since both the improved conventional filter and the proposed filter employ the converted signal to realize high Q factor frequency responses, which result in the reduction of the ASE noise, their performances can be improved greatly comparing to the conventional filter. Unfortunately, owing to a lack of  $2 \times 2$  10:90 coupler in our lab, the improved conventional filter cannot be experimentally implemented. Therefore, in order to compare the theoretical frequency responses of the improved conventional filter with the proposed filter, their poles ( $\kappa g_c L_c$  and  $\kappa_1 \kappa_2 g_c L_c$ ) are both set to be 0.993. We assume that the residual pump signals passing through the TNOF have the same effects, i.e., the power ratios (residual pump power to half summation power of the converted signal after photo-detection) have the same value of the 0.009. With a designed FSR of 18.48 MHz, the theoretical frequency responses according to (5) and (6) are shown in Fig. 6(a) (dotted line) and Fig. 6(b) (solid line), respectively. As can be seen from the Figs. 6(a) and 6(b), the theoretical frequency responses are similar to each other. The shape factor of the improved conventional filter is worse, although its rejection ratio is higher. This is because the two-tap frequency response realized by the direct pump signal and the residual pump signal passing through the TNOF, as can be seen from (6). The overall

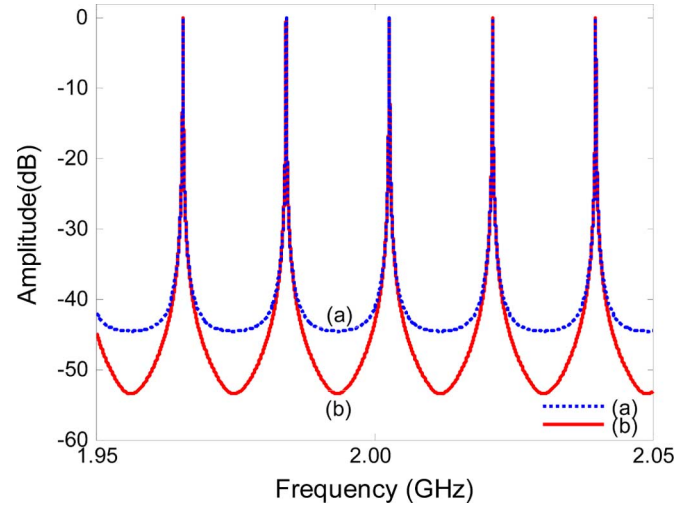


Fig. 6. Theoretical frequency responses of (a) the proposed novel structure, and (b) the improved conventional filter for power ratios of 0.009 with the poles of 0.993.

frequency response is a combination of the two-tap notch frequency response and a high Q factor frequency response with negative coefficients after photo-detection. When a coupler with a given coupling efficient is used, compared with the improved conventional filter, the proposed filter in this paper has the advantage that the pump signal power can be adjusted by tuning the TNOF, which will result in different frequency responses, as shown in Fig. 9.

### III. EXPERIMENTAL RESULTS AND DISCUSSION

The proposed novel filter structure, as shown in Fig. 1, is theoretically analyzed and experimentally implemented/demonstrated. In the proposed filter structure, a  $1 \times 2$  10:90 coupler is used to extract out 10% optical power from the loop rather than using a  $2 \times 2$  coupler to form the loop. Fig. 7 shows the theoretical frequency responses according to (5) for three different power ratios of 0.096, 0.023, and 0.009 with the  $\kappa_1 \kappa_2 L_c g_c$  of 0.993 and a designed FSR of 18.48 MHz. The theoretical shape factor and rejection ratio as the function of the residual pump power are shown in Fig. 8. For convenience, the effective gain of the converted signal is kept constant while the residual pump power varies. As shown in Figs. 7 and 8, both the shape factor and the rejection ratio increase with the reduction of the residual pump power for a given effective gain. The residual pump signal results in a flat band-stop which makes the shape factor better, comparing with the filter frequency response without it. In other words, in the case of the residual pump signal, the  $S$  becomes smaller while the  $B$  keeps constant for a given effective gain, thus the  $S/B$  decreases and the shape factor becomes better.

In this experiment, the total RDL loop length is around 11.18 m, larger than the laser coherent length, and thus the filter structure is operated in the incoherent regime. In addition, since the modulated ASE signal is transmitted in the active loop, its coherent length is very short. Therefore, it is very easy to match the condition of incoherence. This is confirmed by the fact that all the experimental filtering results exhibit very robust and stable

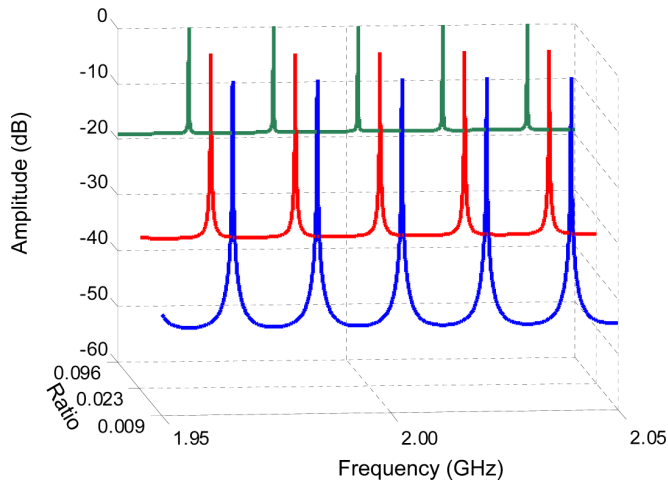


Fig. 7. Theoretical frequency responses for three different power ratios (a) 0.096, (b) 0.023, and (c) 0.009 with the  $\kappa_1\kappa_2L_cg_c$  of 0.993.

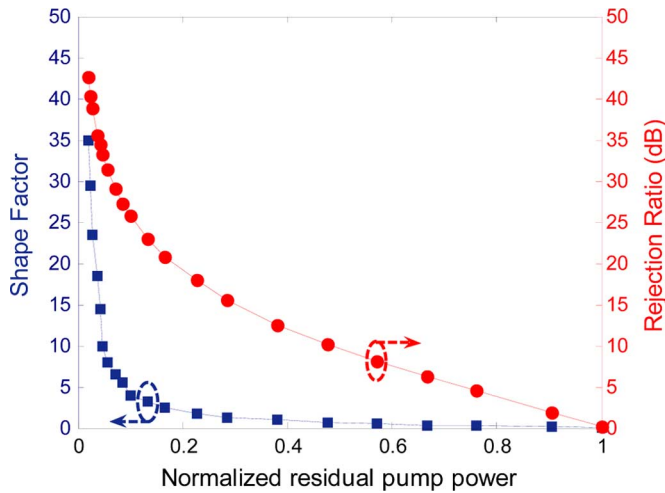


Fig. 8. Theoretical shape factor and rejection ratio for different residual pump power.

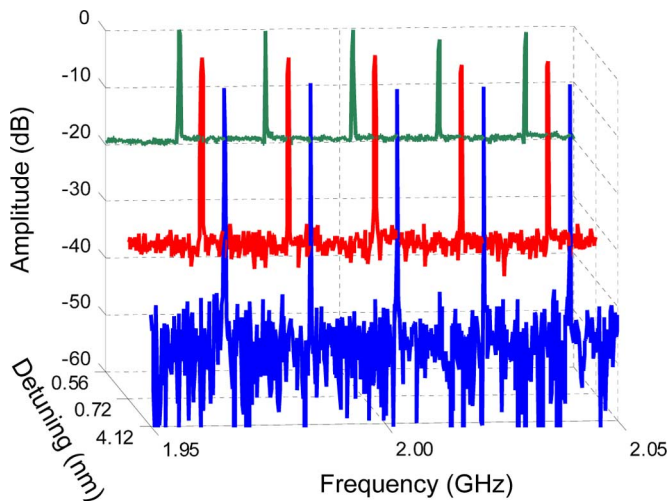


Fig. 9. Measured frequency response for detuning 0.56 nm, 0.72 nm, and 4.12 nm at a given SOA bias current of 52.5 mA for the 10:90 coupler.

characteristics. Accordingly, the FSR is about 18.48 MHz. In

TABLE I  
DETAILED PARAMETERS OF MEASURED RESULTS IN FIG. 9

Detuning (nm)	$\Delta f_{3dB}$ (kHz)	Q factor	Rejection ratio (dB)	Shape factor
0.56	212	84.78	18.68	2.34
0.72	138	133.78	34.92	2.54
4.12	34.04	543.53	40.21	15.40

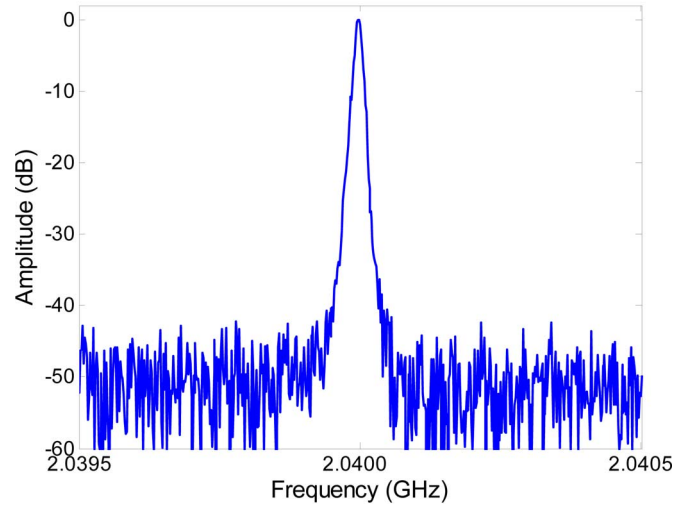


Fig. 10. Zoomed result for detuning 4.12 nm in the Fig. 9.

the case of the SOA biased at 52.5 mA, we observe the variation of the rejection ratio when we adjust the TNOF. Different detuning results in different residual pump power after passing through the TNOF for contributing to the output. Fig. 9 shows the measured frequency responses for three different detuning of the TNOF. As can be seen from Figs. 7 and 9, the measured results are very close to the theoretical results, and the power ratios in Fig. 7 and the detuning in Fig. 9 are in good agreement to each other, that is to say, each detuning has a corresponding residual pump power, and the detailed parameters of the measured results in Fig. 9 are given in Table I.

The zoomed measured frequency response for the detuning of 4.12 nm is shown in Fig. 10. The 3 dB bandwidth is 34.0 kHz, a high Q factor of 543.5 and a rejection ratio of 40.2 dB are achieved, respectively. The 37.2 dB bandwidth is 524.2 kHz, and the shape factor is calculated to be 15.4. It is noted that Q factor, rejection ratio and the shape factor are improved greatly in comparison to the conventional SOA-based bandpass filter structure.

At a given SOA bias current, the rejection ratio is related to the residual pump power, as well as the detuning. The measured Q factor and rejection ratio for different detuning are shown in Fig. 11, and the corresponding shape factor is shown in Fig. 12. As mentioned above, each different detuning has a corresponding residual pump power, and the measured rejection ratios for different detuning are very close to the theoretical rejection ratios for different residual pump powers, as can be seen from Figs. 8 and 11. In fact, at a given SOA bias current, tuning the TNOF will make the optical modulated signals at the pump wavelength and the converted wavelength experience

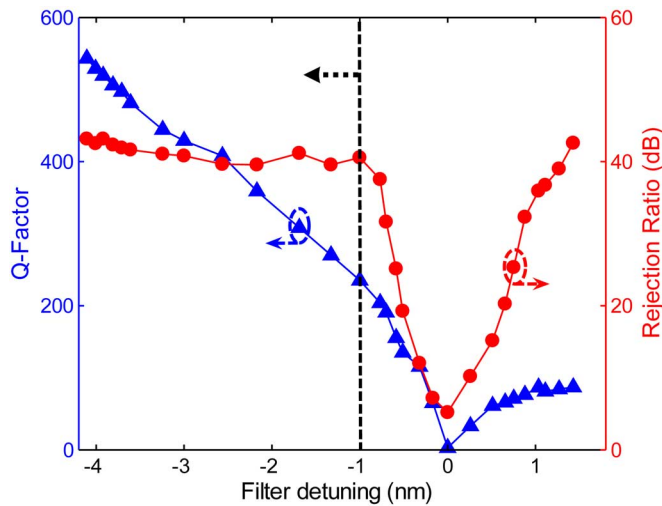


Fig. 11. Measured Q factor and rejection ratio for different detuning.

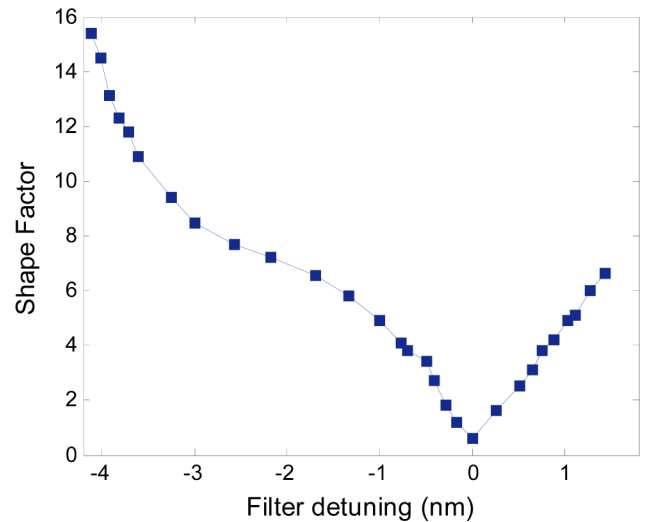


Fig. 12. Measured shape factor for different detuning.

different effective gains, which will induce the change of the Q factor. The Q factor decreases with the reduction of the detuning; the reason is that the residual pump signal power increases with the reduction of the detuning, especially when the detuning is small. A larger residual pump signal depletes much more carriers and suppresses the SOA gain spectrum, making the effective gain of the converted signal reduce. Due to the reduction of the effective gain of the converted signal, the effective number of taps used to implement the bandpass filter is reduced, resulting in a low Q factor. When the central wavelength of the TNOF is aligned with the pump signal wavelength, the Q factor is the minimum. Fig. 11 shows that the rejection ratio varies slightly in the case of larger blue detuning. This is because the residual pump power changes slowly for larger blue detuning, especially when the blue detuning is smaller than the  $-1$  nm, as shown in the region of the left side of the dash line in Fig. 11. Red detuning has a similar characteristic to blue detuning for the Q factor and the rejection ratio. Noting that, the Q factor is not symmetric, this is because the modulated ASE spectrum is not symmetric either at a given SOA bias current, as can be seen from Fig. 2. Therefore, the converted signal will experience different effective gains for red and blue shifts. For the same reason, the rejection ratio is not well symmetric. The sign  $+$  and  $-$  in the x axis represent red and blue detuning, respectively. As can be seen from Fig. 12, the shape factor is better in the case of small detuning, which is similar to the trend of the theoretical shape factor for large residual pump powers, as shown in Fig. 8. This indicates that the shape factor can be better with the help of the residual pump signal, especially in the case of larger residual pump signal as well as smaller detuning. A small difference between the theoretical and experimental results arises from the influence of tuning the TNOF on the changes of the effective gains on the pump signal and converted signal.

We also investigate the Q factor, the rejection ratio and the shape factor versus the SOA bias current in the experiment for the detuning of 4.12 nm. Three measured filter frequency responses for different SOA bias currents are shown in Fig. 13, and the filter performances against the SOA bias current are shown

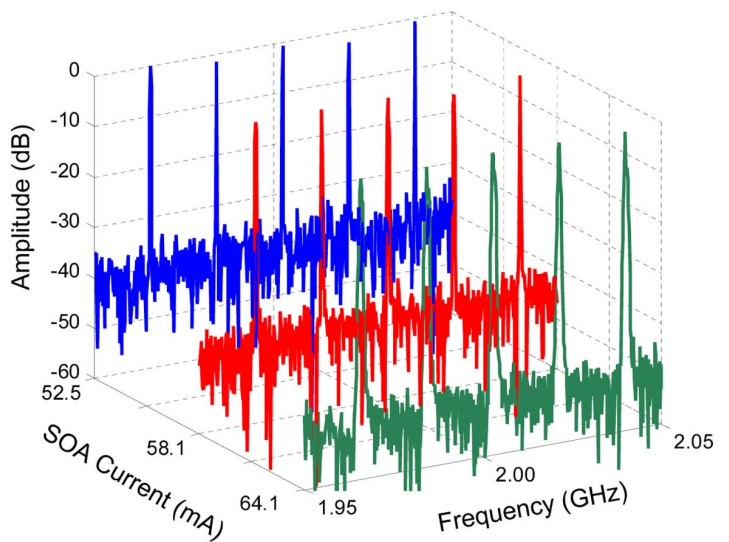


Fig. 13. Measured frequency response for different SOA bias currents.

in Figs. 14 and 15. It can be seen that the Q factor decreases with the increasing of the SOA bias current; our analysis is that the signals on other wavelengths around the central wavelength of the TNOF have effects on the frequency response at larger bias currents when they pass through the filter, and their delay times will be a little different from the basic delay time  $T$  due to the fiber chromatic dispersion.

The rejection ratio increases with the increasing of the SOA bias current due to the SOA effective gain being increased. And the shape factor does not change too much as the current is increased further above 53 mA, as shown in Fig. 15, this is because both the  $B$  and the  $S$  will increase almost the same.

At the output, if the  $1 \times 2$  10:90 optical coupler is substituted by a  $1 \times 2$  40:60 optical coupler, the rejection ratio can be greatly improved. The measured frequency response is shown in Fig. 16. The rejection ratio can be as high as around 53 dB, the 3 dB bandwidth and the FSR are 51.6 kHz and 18.53 MHz, respectively; however, the Q factor is reduced to about 359. Analysis shows that this is due to the change in the SOA gain spec-

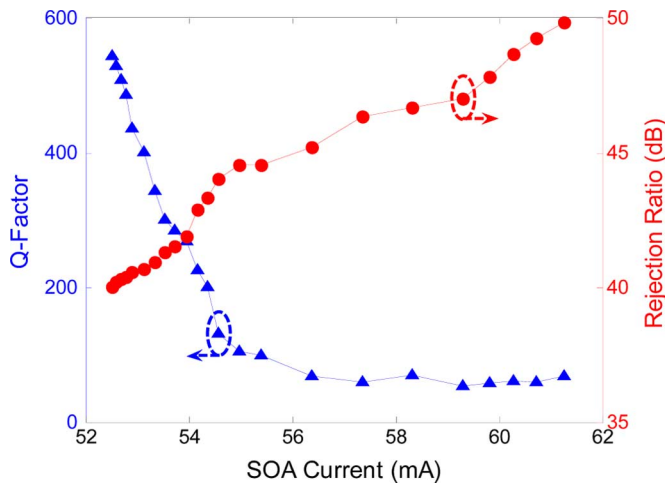


Fig. 14. Measured Q factor and rejection ratio for different SOA bias currents.

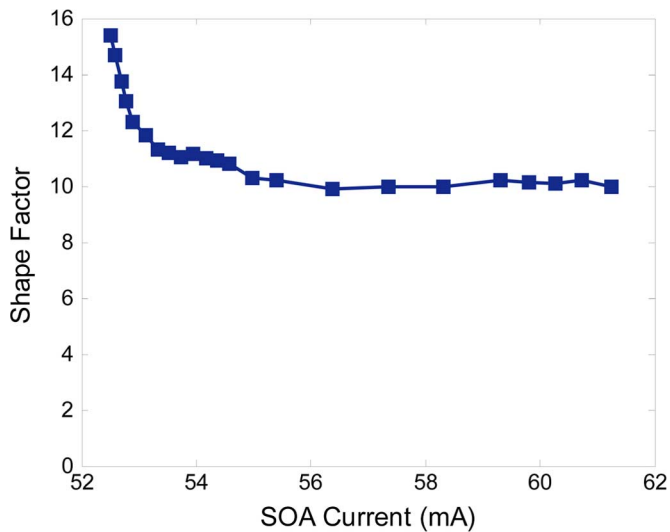


Fig. 15. Measured shape factor for different SOA bias currents.

trum, which results in the variation of the residual pump signal power and the effective gain of the converted signal, making the residual pump signal response power and the attenuated response power of the converted signal be comparable after photo-detection.

Finally, the tuning process can also be realized by tuning the wavelength of a tunable laser diode, which increases the flexibility of the filter. In addition, if the novel filter structure is cascaded with passive filters, the value of the Q factor could be further increased.

#### IV. CONCLUSION

We propose and demonstrate a novel all-optical microwave photonic filter with high frequency selectivity. The filter structure is based on a RDL loop comprising a SOA followed by a TNOF and  $1 \times 2$  10:90 coupler. The converted signal serving as a negative tap is generated employing the XGM of the ASE spectrum of the SOA. The converted signal circulating in the

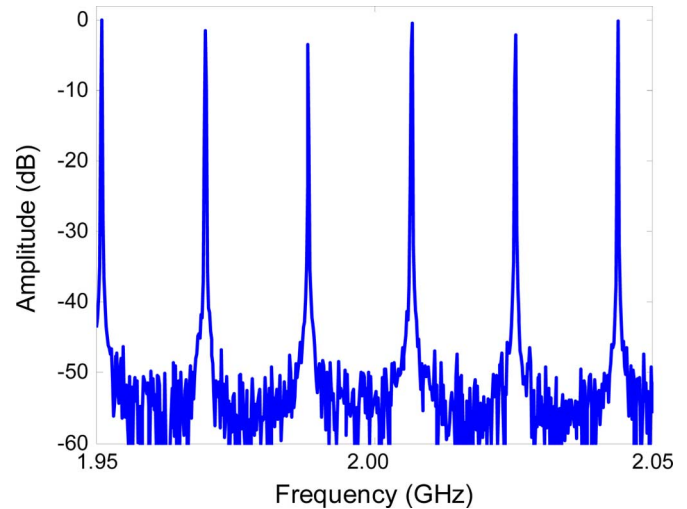


Fig. 16. Measured frequency response for the 40:60 coupler.

RDL loop realizes a high Q factor response with negative coefficients after photo-detection, which is the most important advantage of the structure. A  $1 \times 2$  10:90 coupler is used to extract out 10% optical power as output, being different from the previous conventional bandpass filters in which the optical signal is extracted at the  $2 \times 2$  coupler used to form the loop. The slight all-pass response realized by the small residual pump signal not being filtered out can make the shape factor better. Experimental results have shown a high Q factor of 543, a rejection ratio of 40 dB, and a shape factor of 15.4, greatly improved comparing with the conventional SOA-based bandpass responses. This structure exhibits a very stable operation due to the very short coherent length of the modulated ASE signal. The rejection ratio can be improved by substituting the  $1 \times 2$  10:90 coupler by a  $1 \times 2$  40:60 coupler. By adding an optical variable delay line (OVDL) in the loop, the pass-band frequency of the filter can be tunable. Although the proposed novel filter and the improved conventional filter have the similar frequency response, the proposed novel filter has the advantage that the pump signal power can be adjusted by tuning the TNOF, when a coupler with a given coupling efficient is used, which will result in different frequency response characteristics. Finally, if the novel filter is cascaded with other filters, the value of the Q factor could be further increased.

#### REFERENCES

- [1] J. Yao, "Microwave photonics," *J. Lightw. Technol.*, vol. 27, no. 3, pp. 314–335, Feb. 2009.
- [2] J. Capmany, B. Ortega, and D. Pastor, "A tutorial on microwave photonic filters," *J. Lightwave Technol.*, vol. 24, no. 1, pp. 201–229, Jan. 2006.
- [3] R. A. Minasian, "Photonic signal processing of microwave signals," *IEEE Trans. Microw. Theory Tech.*, vol. 54, no. 2, pp. 832–846, Feb. 2006.
- [4] J. Capmany and D. Novak, "Microwave photonics combines two worlds," *Nature Photonics*, vol. 1, pp. 319–330, Jun. 2007.
- [5] T. X. H. Huang, X. Yi, and R. A. Minasian, "New multiple-tap, general-response, reconfigurable photonic signal processor," *Opt. Exp.*, vol. 17, no. 7, pp. 5358–5363, Mar. 2009.

- [6] M. Sagues, R. G. Olcina, A. Loayssa, S. Sales, and J. Capmany, "Multi-tap complex-coefficient incoherentmicrowave photonic filters based on optical single-sideband modulation and narrow band optical filtering," *Opt. Exp.*, vol. 16, no. 1, pp. 295–303, Jan. 2008.
- [7] Y. T. Dai and J. P. Yao, "Nonuniformly-spaced photonic microwave delay-line filter," *Opt. Express*, vol. 16, no. 7, pp. 4713–4718, Mar. 2008.
- [8] J. Mora, A. Ortigosa-Blanch, D. Pastor, and J. Capmany, "Tunable microwave photonic filter free from baseband and carrier suppression effect not requiring single sideband modulation using a Mach-Zehnder configuration," *Opt. Exp.*, vol. 14, no. 17, pp. 7960–7965, Aug. 2006.
- [9] D. B. Hunter and R. A. Minasian, "Photonic signal processing of microwave signals using an active-fiber bragg-grating-pair structure," *IEEE Trans. Microw. Theory Tech.*, vol. 45, no. 8, pp. 1463–1466, Aug. 1997.
- [10] E. H. W. Chan, K. E. Alameh, and R. A. Minasian, "Photonic bandpass filters with high skirt selectivity and stopband attenuation," *J. Lightw. Technol.*, vol. 20, no. 10, pp. 1962–1967, Oct. 2002.
- [11] E. H. W. Chan and R. A. Minasian, "Reflective amplified recirculating delay line bandpass filter," *J. Lightw. Technol.*, vol. 25, no. 6, pp. 1441–1446, Jun. 2007.
- [12] B. Vidal, M. A. Piqueras, and J. Marti, "Tunable and reconfigurable photonic microwave filter based on stimulated Brillouin scattering," *Opt. Lett.*, vol. 32, no. 1, pp. 23–25, Jan. 2007.
- [13] E. M. Xu, X. L. Zhang, L. N. Zhou, Y. Zhang, and D. X. Huang, "All-optical microwave notch filter with flat passband based on semiconductor optical amplifier," *Opt. Commun.*, vol. 282, no. 12, pp. 2297–2300, Jun. 2009.
- [14] E. M. Xu, X. L. Zhang, L. N. Zhou, Y. Zhang, and D. X. Huang, "A simple microwave photonic notch filter based on a semiconductor optical amplifier," *J. Opt. A Pure Appl. Opt.*, vol. 11, no. 8, pp. 085405–, Aug. 2009.
- [15] X. Yi, F. Wei, N. J. Hong, and L. Chao, "Tunable microwave filter design using wavelength conversion technique and high dispersion time delays," *IEEE Photon. Technol. Lett.*, vol. 13, no. 8, pp. 857–859, Aug. 2001.
- [16] D. M. Liu, N. J. Hong, and L. Chao, "Wavelength conversion based on cross-gain modulation of ASE spectrum of SOA," *IEEE Photon. Technol. Lett.*, vol. 12, no. 9, pp. 1222–1224, Sep. 2000.
- [17] R. Zheng, K. Alameh, Y. T. Lee, and Z. L. Wang, "Multitap coherence-free photonic RF filter employing semiconductor optical amplifier," *Microw. Opt. Technol. Lett.*, vol. 49, no. 5, pp. 1103–1106, May 2007.
- [18] L. N. Zhou, X. L. Zhang, E. M. Xu, and D. X. Huang, "Q value analysis of a first-order IIR microwave photonic filter based on SOA," *Acta Phys. Sin.*, vol. 58, no. 2, pp. 1036–1041, Feb. 2009.

**Enming Xu** is currently working toward the Ph.D. degree in Wuhan National Laboratory for Optoelectronics and the School of Optoelectronic Science and Engineering, Huazhong University of Science and Technology.

His current research interests include microwave photonic, optical signal processing technologies based on semiconductor devices.

**Xinliang Zhang** (M'08) received the Ph.D. degree in physical electronics from Huazhong University of Science and Technology (HUST), Wuhan, China, in 2001.

He is currently with Wuhan National Laboratory for Optoelectronics and the School of Optoelectronic Science and Engineering, HUST, as a Professor. He is the author or coauthor of more than 160 journal and conference papers. His current research interests include all-optical signal processing and related components.

**Lina Zhou** is currently working toward the Ph.D. degree in Wuhan National Laboratory for Optoelectronics and the School of Optoelectronic Science and Engineering, Huazhong University of Science and Technology.

His current research interests include microwave photonic, optical signal processing technologies based on semiconductor devices.

**Yu Zhang** is currently working toward the Ph.D. degree in Wuhan National Laboratory for Optoelectronics and the School of Optoelectronic Science and Engineering, Huazhong University of Science and Technology.

His current research interests include microwave photonic, optical signal processing technologies based on semiconductor devices and microfiber ring resonator.

**Yuan Yu** is currently working toward the Ph.D. degree in Wuhan National Laboratory for Optoelectronics and the School of Optoelectronic Science and Engineering, Huazhong University of Science and Technology.

His current research interests include microwave photonic, optical signal processing technologies based on semiconductor devices.

**Xiang Li** is currently working toward the M.Eng. degree in Wuhan National Laboratory for Optoelectronics and the School of Optoelectronic Science and Engineering, Huazhong University of Science and Technology.

His current research interests include microwave photonic, optical signal processing technologies based on semiconductor devices.

**Dexiu Huang** was born in Hunan Province, China, on October 1937. He received the B.S. degree in physics from Huazhong University of Science and Technology, Wuhan, China, in 1963.

Since 1963, he has been with Huazhong University of Science and Technology earlier as an Assistant Professor, then as a Lecturer and an Associate Professor, and currently, as a Professor and the Dean of School of Optoelectronic Science and Engineering, and the Associate Director of the Wuhan National Laboratory for Optoelectronics. From 1972 to 1981, he was engaged in research on solid-state lasers and applications. During 1981–1983, he was a Visiting Scientist at the Oregon Graduate Center, where he was engaged in research on semiconductor optoelectronic devices. He is the author or coauthor of more than 200 papers and five books: *Semiconductor Optoelectronics* (University Electronic Science and Technology of China Press, 1994), *Semiconductor Lasers and Their Applications* (National Defense Industry Press, 2001), *Introduction of Information Science* (Chinese Electrical Power Press, 2001), *Fiber Optics* (National Defense Industry Press, 1995), and *Fiber Technology and Applications* (University Electronic Science and Technology of China Press, 1995).